# Shear-induced domain deformation in a tilted lipid monolayer: From circle to ellipse and kinked stripe

Mitsumasa Iwamoto,[1] Tetsuya Yamamoto,[1,2] Fei Liu,[3] and Zhong-Can Ou-Yang[3,4]
[1]*Department of Physical Electronics, Tokyo Institute of Technology, 2-12-1 S3-33 O-okayama, Meguro-ku, Tokyo 152-8552, Japan*
[2]*JSPS, 8 Ichibancho, Chiyoda-ku, Tokyo 102-8472, Japan*
[3]*Center of Advanced Study, Tsinghua University, Beijing 100084, China*
[4]*Institute of Theoretical Physics, The Chinese Academy of Science, P.O. Box 2735, Beijing 100080, China*
(Received 19 February 2008; revised manuscript received 19 August 2008; published 18 November 2008)

The shear-induced domain deformation in a lipid monolayer comprised of tilted molecules is studied as a mechanical balance between surface pressure, line tension, electrostatic energy due to the dipole-dipole interaction, hexatic-elastic stress, and viscous stress. It is found that a simple shear can deform a circular domain into an elliptic shape with the long axis inclined 45° from the shear direction. The "ellipse" is elongated in the long axis as shear rate increases, and evolves to a straight or kinked stripe, which was observed as a "shear band" by Fuller's group [Science **274**, 233 (1996)] and "avalanche-like fronts" by Schwaltz's group [Langmuir **17**, 3017 (2001)], at a threshold shear rate. The propagation of stripe-shaped domains is discussed in the context of electrostatic energy. The dependence of the threshold shear rate on surface pressure is predicted in good agreement with observation and can be used to estimate surface viscosity. The shear-induced domain deformation is maintained by the effect of the lattice elastic stress when shear ceases.

DOI: 10.1103/PhysRevE.78.051704 PACS number(s): 61.30.Cz, 68.18.−g, 64.70.−p

The structures of amphiphile monolayers have been studied extensively during the past two decades [1]. Of particular interest are the condensed phases $L_2$ and $L_2'$, in which the polar heads of the constituent amphiphiles are aligned on a deformed hexatic lattice as observed by experiments [2,3] and predicted by theory [4], whereas alkane tails are tilted toward a nearest neighbor (NN) in $L_2$ phase and a next nearest neighbor (NNN) in $L_2'$ phase. During the same period, much work has been devoted to the understanding of the shape and shape transition of condensed phase domains surrounded by a fluid phase [5–10] by considering the competition between the long-range electrostatic force and the line tension at domain boundary, yet without regard to structure knowledge. Recently, it was revealed that domain shapes were dependent on phase structures in condensed phase. In Brewster angle microscopy (BAM) observation in two types of flow, i.e., pure extension and simple shear (Fig. 1), Fuller's group [11–13] found an indication of strong coupling between shear flow, domain shape, and molecular orientation. They found that initially rich mosaic polydomain structure of $L_2'$ phase was annealed by a shear flow more obviously than in $L_2$ phase so that only two orientations either along or against the flow direction are possible. They also found that the reorientation was accompanied by a sudden appearance of new domains in $L_2'$ called "shear bands" with boundaries oriented toward $\pm 45°$ from the extension axis for the extension flow [Fig. 5 (H) in [12]] and either parallel or perpendicular to the flow direction of simple shear flow [Fig. 14 in [13]]. The mechanism of reorientation was argued [11–13] as the flow alignment of bulk nematic liquid crystals (NLCs) proposed by Helfrich [14]. On the other hand, Schwartz's group observed a novel feature in a simple shear flow [15,24,25]: rotational flow [Fig. 1(b)] induced the rotation of an $L_2'$ domain, which is accompanied by a faster rotation of molecular tilt azimuth than the domain rotation, so-called molecular precession (Fig. 2 in [24]). Moreover, they found continuous orientation jump (Fig. 4 in [24]) and argued a different orientation mechanism: the $C_{2v}$ symmetric lines of the pseudohexagonal lattices in $L_2'$ (or $Ov$) phases must align in the flow direction (Fig. 4 in [15]). Recently, the observations of shape relaxation of the shear-stretched domains in Langmuir films have been successfully used to study line tension between the fluid phases [16–19].

Theoretically, there have been several studies of the shape relaxation of fluid domains in Langmuir films by using the general hydrodynamics model [18,20–23], however the essential difference of the phases between the domain boundaries, the $L_2$ and $L_2'$ and isotropic phases, has not been considered in physics. On the other hand, we have investigated the compression-shear-induced azimuth orientation, i.e., a $C_\infty \rightarrow C_{2v}$ transition of a monolayer in tilting phases ($L_2$ and $L_2'$), as mechanical balance between the elastic stress in hexatic alignment and viscous stress of two-dimensional (2D) LC flow [26]. With the same model, we analyzed the shear-induced orientation of $L_2$ and $L_2'$ phases in the pure-extension and simple shear flows [27], and Fuller's and Schwartz's groups have been accounted for on the basis of this model. The predicted steep change of flow orientation (Fig. 3 in [27]) shows beautiful quantitative agreement with the observation (Fig. 4 in [24]). However, our treatment of the problem is still insufficient. Although the "shear band"

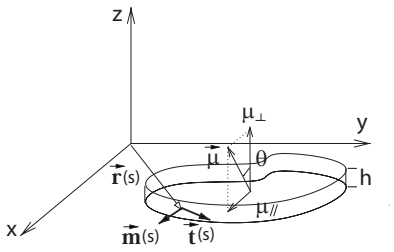


FIG. 1. Two types of flow induced by a four-roll mill used by Fuller's group: (a) a pure extension and (b) a simple shear (after Fig. 1 in Ref. [13]).

 

was discussed by 2D Wulff construction [27], a quantitative analysis for either domain deformation or shear band formation has not been achieved yet.

In this paper, a generalized 2D Young-Laplace equation is derived for a monolayer domain in mechanical balance between the line tension, surface pressure, electrostatic force, elastic stress, and viscous stress. We solved the equation analytically and demonstrated that simple shear flow can deform a circular domain into an elliptic shape with the long axis inclined by 45° from the shear direction. In increasing shear rate, the "ellipse" grows mainly in the direction of the long axis and evolves into straight or kinked stripes at a threshold shear rate. The propagation of stripe domains is also discussed in the context of the electrostatic energy due to the dipole-dipole interaction, which is renormalized to the effective line tension in our previous study [9,10]. The boundary orientation and kink angles of the stripe domains predicted in the present theory are in good agreement with those of the "shear bands" observed by Fuller's group and of the avalanche-like fronts observed by Schwartz's group [25] (see below for details). Especially, the obtained dependence of the threshold shear rate on the surface pressure difference shows quantitative agreement with experimental observation and can be used to estimate the surface viscosity, a classical test in 2D flow. We also show that shear-induced domain deformation including orientation is maintained by the effect of the lattice elastic stress.

## STATICS

In static equilibrium, the shape of a 2D domain is determined by the minimization of the shape free energy [9,10],

$$F = \Delta P \int dA + \lambda \oint ds + F_{\text{dipole}}, \tag{1}$$

where $dA$ and $ds$ are the domain area element and boundary length element, respectively (see Fig. 2). $\lambda$ is the line tension. $\Delta P = \Pi - g_0$, where $\Pi$ is the surface pressure and $g_0$ is the difference of Gibbs free energy density between the outer (isotropic fluid phase) and inner ($L_2$ or $L_2'$) phases. $g_0$ is negative since $L_2$ and $L_2'$ are more condensed than the isotropic fluid phase. $F_{\text{dipole}}$ is the electrostatic energy due to the dipole-dipole interaction. Applying the variational principle ($\delta F = 0$) to the shape free energy, we have derived the shape equation for monolayer domains with uniformly tilted dipole moments as [10]

$$\Delta P - \Lambda\kappa + \alpha\kappa^3 + \beta\kappa_{ss} + \tau\kappa\kappa_s = 0, \tag{2}$$

where $\kappa$ is the curvature of boundary curve, $\kappa_s = d\kappa/ds$, and $\kappa_{ss} = d^2\kappa/ds^2$. The derivation of Eq. (3) is given in the Appendix to be self-contained. $\Lambda$, $\alpha$, $\beta$, $\tau$ are dependent on the molecular tilt angle $\theta$ from the monolayer normal, the dipole density $\mu = \mu_0(\sin\theta, 0, \cos\theta)$, the boundary perimeter $L$, and the boundary azimuth $\phi(s)$, i.e., the angle between the boundary tangent and the in-plane component of the dipole density [see Eqs. (A19)–(A22)]. For example, the effective line tension $\Lambda$, in which the contribution of $F_{\text{dipole}}$ is renormalized, takes the following complex form:

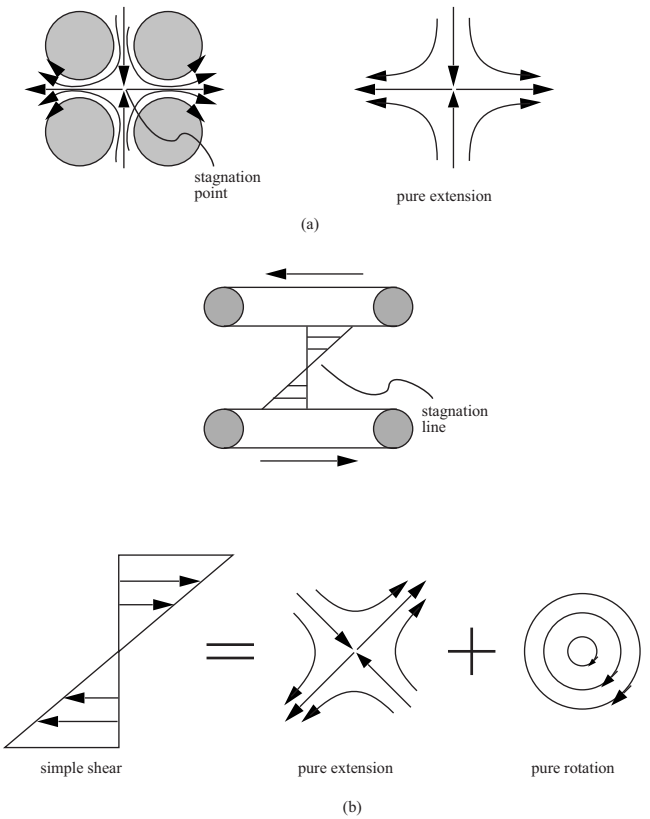


FIG. 2. The geometry of the monolayer domain.

$$\Lambda = \lambda - \frac{\mu_\perp^2}{2}\ln\frac{Le}{h} + \frac{\mu_\parallel^2}{4}(1 + 3\cos 2\phi)\ln\frac{L}{h} + \frac{11}{48}\mu_\perp^2 L\oint ds\kappa^2 + \frac{\mu_\parallel}{2L}\oint ds\sin^2\phi - \frac{1}{96}\mu_\parallel L\oint ds[(11 + 13\cos 2\phi)\kappa^2] \tag{3}$$

with $\mu_\perp = \mu_0\cos\theta$ and $\mu_\parallel = \mu_0\sin\theta$. $h$ is the thickness of the monolayer. Equation (2) represents the mechanical balance of the stress applied at the domain boundary in the normal $\mathbf{m}(s)[=(\sin\phi(s), -\cos\phi(s))]$ of the domain boundary curve (see Fig. 2). The formation mechanism of some complex domain shapes observed in a lipid monolayer has been revealed from the solution of Eq. (2) [10].

## DYNAMICS

In the application of simple shear, straight fronts are suddenly nucleated and are propagated in the direction 45° from the flow direction [15]. This indicates that the fronts are the shape deformation of domains induced by the monolayer hydrodynamics. In the presence of monolayer flows, a part of the work done by the mechanical stresses is dissipated, and viscotic stresses are applied in the monolayers. Domains in monolayers deform their shape to achieve mechanical balance at the domain boundary, i.e.,

$$\Delta P - \Lambda\kappa + \alpha\kappa^3 + \beta\kappa_{ss} + \tau\kappa\kappa_s = \mathbf{m}(s)\cdot(\mathbf{t}^{\text{out}} - \mathbf{t}^{\text{in}})\cdot\mathbf{m}(s). \tag{4}$$

$\mathbf{m}(s) = (\sin\phi(s), -\cos\phi(s))$ is the outward normal vector of the domain boundary curve [Eqs. (7) and (8) in [10]]. $\mathbf{t}^{\text{out}}$ and

$\mathbf{t}^{\text{in}}$ are the outer and inner viscous stress tensors, respectively. This treatment has been used to analyze the fluctuation of vesicles and membranes [28]. The left-hand side of Eq. (4) has been derived for the static monolayer domains with uniformly tilting dipoles, i.e., the left-hand side of Eq. (2). In other words, the shape equation, Eq. (2), is a special case of Eq. (4). The viscous stress from the outside phase is simply written as $t_{ij}^{\text{out}}=\eta d_{ij}$ with $d_{ij}=\frac{1}{2}(v_{j,i}+v_{i,j})$, where $v_{j,i}=\partial v_j/\partial x_i$ ($\mathbf{v}$ is the velocity field in the outside phase) since the outer phase is just an isotropic fluid. $\eta$ is the (isotropic) viscotic coefficient of the outer phase. On account of the tilting of molecular tails, in-plane viscosity of monolayers in $L_2$ and $L_2'$ phases is anisotropic. In a similar manner to our previous studies [26,27], we regard monolayers in these phases as nematic liquid crystals (NLCs) and use the viscotic stress tensor of the Ericksen-Leslie theory of NLCs [29,30]

$$t_{ij}^{\text{in}}=\mu_1 n_i n_j n_k n_l d_{kl}+\mu_2 n_i N_j+\mu_3 n_j N_i+\mu_4 d_{ij}+\mu_5 n_i n_k d_{kj}+\mu_6 n_j n_k d_{ki}, \tag{5}$$

for the representation of the viscous stress applied from the inner phase. The Einstein sum rule is used in the expression. $\mu_1-\mu_6$ are Leslie viscotic coefficients. $\mathbf{n}[=(\sin\theta\cos\gamma,\sin\theta\sin\gamma,\cos\theta)]$ is the average orientation of molecular tails (director) and $\mathbf{N}=d\mathbf{n}/dt-\mathbf{w}\cdot\mathbf{n}$ with $w_{ij}=\frac{1}{2}(v_{j,i}-v_{i,j})$. We assume a simple shear flow in the $x$ direction $[\mathbf{v}=(\dot{\epsilon}y,0)]$ with constant shear rate $\dot{\epsilon}$. The nonvanishing components of $d_{ij}$ and $w_{ij}$ are $d_{12}=d_{21}=\dot{\epsilon}/2$ and $w_{12}=-w_{21}=\dot{\epsilon}/2$. We have shown that the simple shear flow reorients the director toward the direction of $\gamma=\gamma^*$ or $\pi-\gamma^*$ with $\gamma^*=\arctan(\sqrt{\mu_3/\mu_2})$. $\gamma^*$ is small since $|\mu_3|\ll|\mu_2|$ (e.g., $\gamma^*=10°$ for $p$-azoxyanisoble [14]), which is in agreement with the observation by Fuller's group. For simplicity, we assume $\gamma^*=0$ in the following. In the steady state ($d\mathbf{n}/dt=0$), $\mathbf{N}=-\mathbf{w}\cdot\mathbf{n}$. The normal tensile component of viscous stress from the inner phase is calculated as $\mathbf{m}\cdot\mathbf{t}^{(\text{in})}\cdot\mathbf{m}=-\frac{\dot{\epsilon}}{2}[\mu_4+\frac{1}{2}(\mu_2+\mu_3+\mu_5+\mu_6)\sin^2\theta]\sin 2\phi(s)$. It is further reduced to $\mathbf{m}\cdot\mathbf{t}^{(\text{in})}\cdot\mathbf{m}=-\frac{\dot{\epsilon}}{2}\mu_4\sin 2\phi(s)$ since $\mu_4\gg|\mu_2+\mu_3+\mu_5+\mu_6|$ is usually satisfied [29,30].

As a first approximation, we neglect the contribution of the electrostatic energy for the moment, where $\mu_0=0$ was stated for the experiment carried out by Fuller's group [13] (p. 1839). We will discuss the contribution of the electrostatic energy later. On this assumption, Eq. (4) is reduced to

$$\Delta P+\lambda\frac{d\phi}{ds}=\frac{\dot{\epsilon}}{2}\Delta\mu_4\sin 2\phi \tag{6}$$

with $\Delta\mu_4=\mu_4-\eta$. $\Delta\mu_4$ is positive since the inner phase is more condensed than the outer phase. $\kappa=-d\phi/ds$ was used to derive Eq. (6). The solution of Eq. (6) is derived straightforwardly as

$$\tan\phi(s)=\cos\omega_1\tan\left(\frac{s\cos\omega_1}{\rho_0}+\omega_1\right)-\sin\omega_1 \tag{7}$$

for $|\sin\omega_1|<1$ ($\sin\omega_1=\dot{\epsilon}\Delta\mu_4\rho_0/2\lambda$), and

$$\tan\phi(s)=\sinh\omega_2\tan\left(\frac{s\sinh\omega_2}{\rho_0}\right)-\cosh\omega_2 \tag{8}$$

for $|\cosh\omega_2|>1$ ($\cosh\omega_2=\dot{\epsilon}\Delta\mu_4\rho_0/2\lambda$). $\rho_0=\lambda/(-\Delta P)$. Without loss of generality, we chose $\phi(0)=0$ for Eq. (7) and $\phi(0)=-\cosh\omega_2$ for Eq. (8).

Using $dy/dx=\tan\phi$ and the most simple software, i.e., MATHEMATICA, we calculated a series of domain (or front) shapes for Eqs. (7) and (8) as shown in Figs. 3(a) and 3(b), respectively. Figure 3(a) reveals that monolayers form a circular domain with radius $\rho_0$ when $\dot{\epsilon}=0$, and that the circular domain is deformed into an elliptic domain with the long axis inclined by $\pm45°$ from the flow direction, i.e., the $x$ axis, for $\dot{\epsilon}<0$ and $\dot{\epsilon}>0$, respectively, as $|\dot{\epsilon}|$ increases. The circular domain is also deformed into elliptic domains in the case of $\gamma=\pi$, and the long axis is inclined by $\mp45°$ from the flow direction for $\dot{\epsilon}<0$ and $\dot{\epsilon}>0$, respectively. The angle can be approved by the so-called four-vertices theorem [31]: A closed and smooth planar curve has at least four vertices at which curvature is extremal ($\kappa_s=0$). From Eq. (6), we have $\kappa_s=(\dot{\epsilon}\Delta\mu_4/\lambda)\kappa\cos 2\phi$, i.e., $\phi=\pi/4,3\pi/4,5\pi/4,7\pi/4$ at vertices, and the corresponding normal azimuth $\phi'=\phi-\pi/2=-\pi/4,\pi/4,3\pi/4,5\pi/4$. The shear deformation of domain shapes from a circle to an inclined ellipse was reported early in experiment (Fig. 1b in [8]). The present theory clarified for the first time the mechanism of the shear domain deformation analytically. The most important feature of Fig. 3 is that the elliptic shape grows in size mainly in the direction of the long axis. The growth of type-I fronts in $L_2'$ phase agreed with the growth of two elliptic shapes inclined by $-45°$ from the $x$ axis (see inclined boundaries of the bright domains of Fig. 6 in [25]) at $\dot{\epsilon}=-0.26\ \text{s}^{-1}$, obviously with $\gamma^*=\pi$.

Much to our surprise are the solutions of Eq. (8). At the threshold shear, $\omega_2=0$, Eq. (8) gives a straight stripe with boundaries oriented in $\phi=\pi/4$ and $\phi=3\pi/4$ [in Fig. 3(b) we only showed one of them]. As $\omega_2$ value increases from the threshold, the stripe domain develops a kink at which two straight stripes cross. Each of the two stripes has boundaries oriented in $\phi(-\infty)=\pi-\arctan e^{-\omega_2}$ and $\phi(\infty)=\pi-\arctan e^{\omega_2}$. Obviously, the kink angle $\phi(\infty)-\phi(-\infty)$ increases with $|\dot{\epsilon}|$ from 0 ($\omega_2=0$) to $\pi/2$ ($\omega_2=\infty$): actually, the kink angle is already very close to $\pi/2$ when $\omega_2=4$ [in Fig. 2(b)]. Later, we show the "shear band" observed by the Fuller group [12] being the case of stripe domains with a kink angle of $\pi/2$. The propagation of avalanche-like fronts (type-II fronts) observed by the Schwartz group (Fig. 7 in [25]) agrees with the stripe domains with a kink angle of 30° in $L_2'$ at $T=17\ °\text{C}$, $\Pi=23\ \text{mN/m}$, and $\dot{\epsilon}=-0.55\ \text{s}^{-1}$ reproduced in the present study. The threshold surface pressure $\Pi_{\text{th}}$ is derived from the condition of $\cosh\omega_2>1$ as

$$\Pi>g_0-\frac{1}{2}|\dot{\epsilon}|\Delta\mu_4\equiv\Pi_{\text{th}}(\dot{\epsilon}), \tag{9}$$

where type-II fronts form. Equation (9) shows nice agreement with the experimental results of the $\Pi$-$\dot{\epsilon}$ "phase diagram" (Fig. 3 in [25]), where $\Pi_{\text{th}}$ is a decreasing function of $\dot{\epsilon}$. We roughly estimated the surface viscosity $\Delta\mu_4$ from the

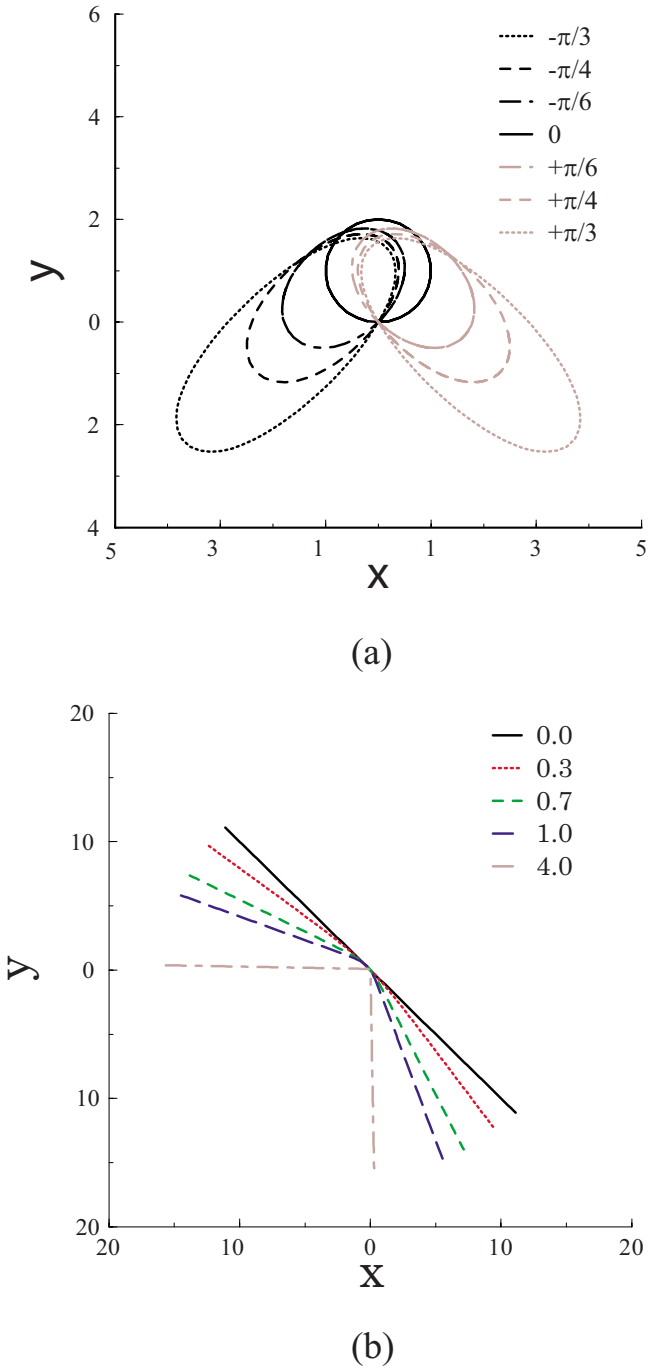


FIG. 3. (Color online) Two types of shear-induced domain shape transition. (a) The case of weak shear; circle to elliptic shape transition calculated by Eq. (6) with indicated $\omega_1$ values. (b) The case of strong shear; a straight stripe domain is formed at the threshold shear rate ($\omega_2=0$), and the stripe domain develops a kink as $\omega_2$ increases.

tangent of $\Pi(C+F+A)-\dot{\epsilon}$ curve at $|\dot{\epsilon}|=0.6\ \mathrm{s}^{-1}$ in the diagram as $\Delta\mu_4=0.3\ \mathrm{gs}^{-1}$. The decrease of the tangent of the $\Pi$-$\dot{\epsilon}$ indicates that $\Delta\mu_4$ decreases as $\dot{\epsilon}$ increases (shear thinning), which is in good agreement with the classical viscosity measurement in a channel flow (Fig. 8 in [32]).

## SHEAR BANDS AND DIPOLE FORCE EFFECT

The above results in simple shear flow are valid in pure extension flow with $\mathbf{v}=(\dot{\epsilon}x,-\dot{\epsilon}y)$ [Fig. 1(a)]. $d_{11}=-d_{22}=\dot{\epsilon}$ are the only nonzero components of $d_{ij}$ and $w_{ij}$ of pure extension flow. The nonzero component of the viscous stress tensor is $t_{11}^{\mathrm{in}}=[\mu_1\sin^2\theta+(\mu_5+\mu_6)\sin^2\theta+\mu_4]\dot{\epsilon}\sim\mu_4\dot{\epsilon}$ and $t_{22}^{\mathrm{out}}=-\mu_4\dot{\epsilon}$. Therefore, the shape equation of monolayer domains in pure extension flow is derived as

$$\Delta P+\lambda\frac{d\phi}{ds}=\frac{\dot{\epsilon}}{2}\Delta\mu_4\cos 2\phi. \tag{10}$$

In the variable transformation $\varphi(s)=\phi(s)+\pi/4$, Eq. (10) is rewritten as $\Delta P+\lambda\frac{d\varphi}{ds}=\frac{\dot{\epsilon}}{2}\Delta\mu_4\sin 2\varphi$, which is the same as Eq. (6). In other words, the solution of Eq. (10) is derived by turning the solution of Eq. (6) by 45°. The shear bands observed by Fuller's group in $L_2'$ [Fig. 5 (B) and (H) in [12]] are just the stripe domain with a kink angle of $\pi/2$ [see Fig. 3(b)] rotated by 45° in the clockwise direction. The only remaining question is why shear bands are observed only in $L_2'$ but not in $L_2$. In order to answer this question, we must go back to the general equation, Eq. (4), to take into account the electrostatic force due to the dipoles in the domains. It is possible to neglect the contribution of the higher-rank terms of $\kappa$ to the shape equation, i.e., the third, fourth, and fifth terms of Eq. (2), when the domain shape is close to the kinked stripe, where $\kappa\to 0$, and the electrostatic dipolar force contributes as the effective line tension, which is expressed as Eq. (3). In other words, the contribution of the electrostatic dipolar force is taken into account by just changing $\lambda$ to $\Lambda$. The effective line tension is calculated as $\Lambda=\lambda-(\frac{\mu_\perp^2}{2}-\frac{\mu_\parallel^2}{4})\ln\frac{Le}{h}$. The boundary length is enhanced when the $\Lambda$ value is negative, i.e.,

$$\theta=\arctan\frac{\mu_\parallel}{\mu_\perp}<\arctan\sqrt{2}=54.7^\circ=\theta_M. \tag{11}$$

In our previous study, we discussed that $F_{\mathrm{dipole}}=0$ at the magic tilt angle $\theta_M$ for circular domains. Experimentally, $\theta>\theta_M$ was generally satisfied in $L_2$, e.g., $\theta=60°$ was found in an eicosanoic acid monolayer by Durbin *et al.* [2]. The material used in [11–13] is docosanoic acid, the same kind used by Durbin *et al.*, and its tilt in $L_2$ cannot satisfy Eq. (11). This may be the reason for the absence of a shear band in $L_2$.

## HEXATIC ELASTIC STRESS

In the above discussion, we have not taken into account the elastic stress due to the deformation of a hexatic lattice. Hexatic lattice structures of molecular heads are deformed by the tilting of constituent molecules, and the internal elastic stresses $\sigma$ associated with the lattice deformation also take part in the mechanical balance at the domain boundary as

$$\Delta P-\Lambda\kappa+\alpha\kappa^3+\beta\kappa_{ss}+\tau\kappa\kappa_s=\mathbf{m}(s)\cdot(\mathbf{t}^{\mathrm{out}}-\mathbf{t}^{\mathrm{in}}-\sigma)\cdot\mathbf{m}(s). \tag{12}$$

Since the lattice deformation originates from tilting of constituent molecules, the elastic stress tensor is determined by the orientation of the director as [26,27]

$$\sigma_{11,22} = \frac{1}{2}\{K \pm \mu[\cos 2\Phi \cos 2(\Phi - \gamma) + 2 \sin 2\Phi \sin 2(\Phi - \gamma)]\}\tan^2\theta, \quad (13)$$

$$\sigma_{12} = \sigma_{21} = \frac{1}{2}\{\mu[2 \sin 2\Phi \cos 2(\Phi - \gamma) - \cos 2\Phi \sin 2(\Phi - \gamma)]\}\tan^2\theta, \quad (14)$$

where + and − in the square brackets in Eq. (13) are applied to $\sigma_{11}$ and $\sigma_{22}$, respectively. $\theta$ and $\gamma$ are the tilt angle and tilt azimuth of director $\mathbf{n}$. $\Phi$ is the angle between the $x$ axis and the *NN* direction of the hexatic lattice. $K$ and $\mu$ are the plane compression modulus and shear modulus, respectively [33]. In a simple flow, we have assumed $\gamma=0$ (or $\pi$) due to the flow orientation. Therefore, $\Phi=0$ for $L_2$ and $\Phi=\pi/2$ for $L_2'$. This reduces Eqs. (13) and (14) to $\sigma_{11}=\sigma_{22}=\frac{1}{2}[K \pm \mu]\tan^2\theta$ and $\sigma_{12}=\sigma_{21}=0$ for both $L_2$ and $L_2'$. Neglecting the dipolar force, we derive a new shape equation for simple shear flow,

$$\Delta P^* + \lambda \frac{d\varphi^*}{ds} = C \sin 2\varphi^*, \quad (15)$$

with $\Delta P^* = \Delta P + \frac{1}{2}K \tan^2\theta$ and $\varphi^* = \phi + \phi^*$. $\phi^* = \frac{1}{2}\arcsin[\frac{1}{2}\mu \tan^2\theta / C]$ and $C = \frac{1}{2}\sqrt{(\dot{\epsilon}\Delta\mu_4)^2 + (\mu \tan^2\theta)^2}$. In a similar manner to the previous treatment, the solution of Eq. (15) is derived by rotating the solution of Eq. (6) by $\phi^*$ in the clockwise direction. Equation (15) indicates that domains with a hexatic lattice form elliptic shapes, kinked stripe shapes, and shear bands in a simple shear, and that the domain shapes remain even after the flow is stopped ($\dot{\epsilon}=0$) but all turn 45° from the solution of Eq. (6) ($\phi^*=\pi/4$ for $\dot{\epsilon}=0$). In other words, the long axis of the elliptic domain induced by pure elastic stress is oriented perpendicular to the tilt direction ($x$ axis) for $\mu>0$ or parallel to the tilt direction for $\mu<0$. Thus far, it has been considered that the elliptic shape of monolayer domains, e.g., Fig. 5 in [7] and Fig. 4 in [34], originated from electrostatic dipolar force. Our present analysis indicates the possibility that the formation of an elliptic shape is ascribed to the elastic stress of the deformed hexatic lattice. The sharpness of the kink angle is a common feature of kinked stripe domains; it is induced by the elastic stress. The reported value of the inner kink angle $100 \pm 10°$ [35] is well within the range of our prediction [Fig. 3(b)].

## SUMMARY

We have analyzed the shape transition of monolayer domains comprised of dipolar molecules tilted from the water surface normal under shear flow on the basis of mechanical balance of forces. The calculated results predict two types of transition: (i) In a weak shear ($\dot{\epsilon} < \dot{\epsilon}_{\rm th}$), a circular domain is deformed to an elliptic domain, growing in size in the long axis, and with certain inclined angle dependent on shear type. (ii) In a strong shear ($\dot{\epsilon} > \dot{\epsilon}_{\rm th}$), straight or kinked stripe domains are formed [$\dot{\epsilon}_{\rm th} = 2\lambda/(\Delta\mu_4\rho_0)$]. The domain shapes induced by shear flow remain after the flow is stopped due to the coupling between the shear-induced orientation and the lattice elastic stress. We believe that the shear-induced self-assembled domains may be significant for the bottom-up design of the 2D device.

## ACKNOWLEDGMENTS

This work is financially supported by a Grant-in-Aid for Scientific Research (A) (No. 19206034) from the Ministry of Education, Culture, Sports, Science, and Technology (MEXT). T.Y. acknowledges financial support in the form of a Grant-in-Aid for Scientific Research from the Japan Society for the Promotion of Science (JSPS).

## APPENDIX A: DERIVATION OF EQ (3)

Here, we outline the derivation of Eqs. (2) and (3). The derivation of these equations is given in detail in [10]. We derive the shape equation, Eq. (2), by applying the variational principle to the free energy, Eq. (1). The electrostatic energy $F_{\rm dipole}$ arising from dipole-dipole interaction is written as [5]

$$F_{\rm dipole} = -\frac{\mu_\perp^2}{2}\oint\oint \frac{\mathbf{t}(l)\cdot\mathbf{t}(s)}{|\mathbf{r}(l)-\mathbf{r}(s)|}dlds + \frac{\mu_\parallel^2}{2}\oint\oint \frac{[\mathbf{t}(l)\cdot\hat{y}_0][t(s)\cdot\hat{y}_0]}{|\mathbf{r}(l)-\mathbf{r}(s)|}dlds, \quad (A1)$$

where $\mathbf{r}(s)$ and $\mathbf{t}(s)$ are positional and tangent vectors of the domain boundary curve. $s$ ($l$) are the length parameter of the boundary curve and $ds$ ($dl$) are line elements. The first and second terms are the contributions of the normal and in-plane components of dipole moments, respectively. Equation (A1) expresses nonlocal interaction between electric dipoles, where it is represented by the double line integral, and it is difficult to find the shapes of minimal free energy in general. We approximate the free energy on the basis of the Frenet-Seret theorem.

The derivatives of $\mathbf{r}(s)$, $\mathbf{t}(s)$, and $\mathbf{m}(s)$ are given by the Frenet-Seret theorem, and are represented as

$$\frac{d}{ds}\mathbf{r}(s) = \mathbf{t}(s), \quad (A2)$$

$$\frac{d}{ds}\mathbf{t}(s) = \kappa(s)\mathbf{m}(s), \quad (A3)$$

$$\frac{d}{ds}\mathbf{m}(s) = -\kappa(s)\mathbf{t}(s) \quad (A4)$$

by the curvature $\kappa(s)$ of the boundary curve. It indicates that Taylor expansions of $\mathbf{r}(s)$ and $\mathbf{t}(s)$ are possible as

$$\mathbf{r}(s+x) = \mathbf{r}(s) + \mathbf{t}(s)x + \frac{1}{2}\kappa(s)\mathbf{m}(s)x^2 + \frac{1}{6}[\kappa_s(s)\mathbf{m}(s) - \kappa(s)^2\mathbf{t}(s)]x^3 + \cdots \quad (A5)$$

and

$$\mathbf{t}(s+x) = \mathbf{t}(s) + \kappa(s)\mathbf{m}(s)x + \frac{1}{2}[\kappa_s(s)\mathbf{m}(s) - \kappa(s)^2\mathbf{t}(s)]x^2 + \cdots \tag{A6}$$

with $\kappa_s = d\kappa(s)/ds$ and $\kappa_{ss} = d^2\kappa(s)/ds^2$.

The key step to approximate the double line integrals is to rewrite the energies of the two components of the dipole moment as

$$F_{\text{dipole}} = -\frac{\mu_\perp^2}{2}\oint\left[\oint \frac{\mathbf{t}(s)\cdot\mathbf{t}(s+x)}{|\mathbf{r}(s+x)-\mathbf{r}(s)|}dx\right]ds + \frac{\mu_\parallel^2}{2}\oint\left[\oint \frac{[\mathbf{t}(s+x)\cdot\hat{y}_0][\mathbf{t}(s)\cdot\hat{y}_0]}{|\mathbf{r}(s+x)-\mathbf{r}(s)|}dx\right]ds, \tag{A7}$$

where the range of arc-variable $x \equiv l - s$ is $[h, L]$, and $h$ represents a nonzero monolayer thickness, which serves as a cutoff length of the line integrals (see Fig. 2). Using Eqs. (A5) and (A6), the integrand of Eq. (A7) is expanded in a power series of $x$, and the coefficients are dependent on the powers of the curvature $\kappa(s)$, the angle $\phi(s)$, and their derivatives. If we omit the higher-rank terms than the first order of $x$, after integral in terms of $x$, we obtain their approximate expressions as

$$F_\perp \approx -\frac{\mu_\perp^2}{2}\ln\frac{L}{h}\oint ds + \frac{11}{96}\mu_\perp^2 L^2\oint \kappa^2(s)ds \tag{A8}$$

and

$$F_\parallel \approx \frac{\mu_\parallel^2}{2}\ln\frac{L}{h}\oint \sin^2\phi(s)ds - \frac{1}{192}\mu_\parallel^2 L^2\oint [11 + 13\cos 2\phi(s)]\kappa^2(s)ds, \tag{A9}$$

where $F_\perp$ and $F_\parallel$ are the first and second terms of Eq. (A7), respectively ($F_{\text{dipole}} = F_\perp + F_\parallel$). We use Eqs. (A8) and (A9) for the electrostatic energy arising from dipole-dipole interaction in the following calculation. Note that Eq. (A8) is expressed in the form of the sum of the effective negative line tension and the curvature elastic energy.

The shape equation is derived as the equilibrium condition ($\delta^{(1)}F = 0$) of the shape free energy with respect to the shape variations $\mathbf{r}(s) \to \mathbf{r}'(s') = \mathbf{r}(s) + \psi(s)\mathbf{m}(s)$. The line elements of domain boundary $ds'$, tangent vector $\mathbf{t}(s')$, normal vector $\mathbf{m}(s')$, and curvature $\kappa'(s')$ of the domain boundary after the shape variation are represented as

$$ds' = [1 - \kappa(s)\psi(s)]ds, \tag{A10}$$

$$\mathbf{t}'(s') = \mathbf{t}(s) + \psi_s(s)\mathbf{m}(s), \tag{A11}$$

$$\mathbf{m}'(s') = \mathbf{m}(s) - \psi_s(s)\mathbf{t}(s), \tag{A12}$$

$$\kappa'(s') = \kappa(s) + \kappa^2(s)\psi + \psi_{ss}, \tag{A13}$$

respectively. The first variation of each term of Eq. (1) is calculated as

$$\Delta P\delta^{(1)}\int dA = \Delta P\int \psi(s)ds, \tag{A14}$$

$$\lambda\delta^{(1)}\oint ds = \lambda\oint \kappa\psi(s)ds, \tag{A15}$$

$$\delta^{(1)}F_\perp = -\frac{\mu_\perp^2}{2}\oint\left(\frac{11}{24}L\oint \kappa(x)^2dx - \ln\frac{Le}{h}\right)\kappa\psi(s)ds + \frac{11}{96}\mu_\perp^2 L^2\left[\oint \kappa^3\psi(s)ds + 2\oint \kappa_{ss}\psi(s)ds\right], \tag{A16}$$

$$\delta^{(1)}F_\parallel = -\frac{\mu_\parallel^2}{2}\oint\left[\frac{1}{L}\oint \sin^2\phi(x)dx - \frac{11}{48}L\oint \kappa(x)^2dx - \frac{13}{48}L\oint \cos 2\phi\kappa(x)^2dx + \frac{1+3\cos 2\phi(s)}{2}\ln\frac{L}{h}\right]\kappa\psi(s)ds + \mu_\parallel^2 L^2\oint \frac{39\cos 2\phi(s) - 11}{192}\kappa^3\psi(s)ds - \frac{13}{24}\mu_\parallel^2 L^2\oint \sin 2\phi\kappa\kappa_s\psi(s)ds - \mu_\parallel^2 L^2\oint \frac{39\cos 2\phi(s) + 11}{96}\kappa_{ss}\psi(s)ds. \tag{A17}$$

If curve $\vec{r}(s)$ describes a boundary of equilibrium domain, it satisfies $\delta^{(1)}F = 0$ for any infinitesimal function $\psi(s)$. Hence combining Eqs. (A14)–(A17), we get the shape equilibrium condition of the domain,

$$\Delta P - \Lambda\kappa + \alpha\kappa^3 + \beta\kappa_{ss} + \tau\kappa\kappa_s = 0, \tag{A18}$$

where the definitions of the coefficients are

$$\Lambda = \lambda - \frac{\mu_\perp^2}{2}\ln\frac{Le}{h} + \frac{\mu_\parallel^2(1+3\cos 2\phi)}{4}\ln\frac{L}{h} + \frac{11}{48}\mu_\perp^2 L\oint \kappa(s)^2ds + \frac{\mu_\parallel^2}{2L}\oint \sin^2\phi(s)ds - \frac{1}{96}\mu_\parallel^2 L\oint (11 + 13\cos 2\phi)\kappa(s)^2ds, \tag{A19}$$

$$\alpha = \frac{11}{96}\mu_\perp^2 L^2 + \mu_\parallel^2 L^2\frac{39\cos 2\phi - 11}{192}, \tag{A20}$$

$$\beta = \frac{11}{48}\mu_\perp^2 L^2 - \mu_\parallel^2 L^2\frac{11 + 13\cos 2\phi}{96}, \tag{A21}$$

$$\tau = -\frac{13}{24}\mu_\parallel^2 L^2\sin 2\phi. \tag{A22}$$

[1] V. M. Kaganer, H. Mohwald, and P. Dutta, Rev. Mod. Phys. **71**, 779 (1999).
[2] K. Kjaer, J. Als-Nielsen, C. A. Helm, L. A. Laxhuber, and H. Mohwald, Phys. Rev. Lett. **58**, 2224 (1987); P. Dutta, J. B. Peng, B. Lin, J. B. Ketterson, M. Prakash, P. Georgopoulos, and S. Enrlich, *ibid.* **58**, 2228 (1987); M. K. Durbin *et al.*, J. Chem. Phys. **106**, 8216 (1997).
[3] J. Als-Nielsen and H. Möhwald, in *Handbook of Synchrotron Radiation*, edited by S. Ebashi, M. Koch, and E. Rubenstein (Elsevier Science, Amsterdam, 1991), Vol 4, Chap. 1, p. 1.
[4] D. R. Nelson and B. I. Halperin, Phys. Rev. B **21**, 5312 (1980).
[5] D. Andelman, F. Brochard, P. G. de Gennes, and J. F. Joanny, C. R. Acad. Sci. III **301**, 675 (1985); D. Andelman, F. Brochard, and J. F. Joanny, J. Chem. Phys. **86**, 3673 (1987).
[6] R. M. Weis and H. M. McConnell, Nature **310**, 47 (1984); H. E. Gaub, V. T. Moy, and H. M. McConnell, J. Phys. Chem. **90**, 1721 (1986).
[7] D. Keller, J. P. Korb, and H. M. McConnell, J. Phys. Chem. **91**, 6417 (1987).
[8] D. J. Benvegnu and H. M. McConnell, J. Phys. Chem. **96**, 6820 (1992).
[9] M. Iwamoto and Z. C. Ou-Yang, Phys. Rev. Lett. **93**, 206101 (2004).
[10] M. Iwamoto, F. Liu, and Z. C. Ou-Yang, J. Chem. Phys. **125**, 224701 (2006).
[11] M. C. Friedenberg, G. G. Fuller, C. W. Frank, and C. R. Robertson, Langmuir **12**, 1594 (1996).
[12] T. Maruyama, G. Fuller, C. Frank, and C. Robertson, Science **274**, 233 (1996).
[13] T. Maruyama, J. Lauger, G. G. Fuller, C. W. Frank, and C. R. Robertson, Langmuir **14**, 1836 (1998).
[14] W. Helfrich, J. Chem. Phys. **50**, 100 (1969).
[15] J. Ignes-Mullol and D. K. Schwartz, Phys. Rev. Lett. **85**, 1476 (2000).
[16] J. R. Wintersmith, L. Zou, A. J. Bernoff, J. C. Alexander, J. A. Mann, Jr., E. E. Kooijman, and E. K. Mann, Phys. Rev. E **75**, 061605 (2007).
[17] E. K. Mann, S. Henon, D. Langevin, J. Meunier, and L. Leger, Phys. Rev. E **51**, 5708 (1995).
[18] J. C. Alexander, A. J. Bernoff, E. K. Mann, J. A. Mann, Jr., J. R. Wintersmith, and L. Zou, J. Fluid Mech. **571**, 191 (2007).
[19] M. N. G. de Mul and J. A. Mann, Jr., Langmuir **10**, 2311 (1994).
[20] J. C. Alexander, A. J. Bernoff, E. K. Mann, J. A. Mann, and L. Zou, Phys. Fluids **18**, 062103 (2006).
[21] T. Hou, J. Lowengrub, and M. Shelley, J. Comput. Phys. **114**, 312 (1994).
[22] D. K. Lubensky and R. E. Goldstein, Phys. Fluids **8**, 843 (1996).
[23] P. Heinig, L. E. Helseth, and T. M. Fischer, New J. Phys. **6**, 189 (2004).
[24] J. Ignes-Mullol and D. K. Schwartz, Nature **410**, 348 (2001).
[25] J. Ignes-Mullol and D. K. Schwartz, Langmuir **17**, 3017 (2001).
[26] M. Iwamoto, A. Tojima, T. Manaka, and O. Y. Zhong-can, Phys. Rev. E **67**, 041711 (2003).
[27] M. Iwamoto and O. Y. Zhong-can, Phys. Rev. E **72**, 021704 (2005).
[28] S. Komura and K. Seki, Physica A **192**, 27 (1993).
[29] P. G. de Gennes and J. Prost, *The Physics of Liquid Crystals* (Clarendon, Oxford, 1995).
[30] S. Chandrasekhar, *Liquid Crystal*, 2nd ed. (Cambridge University Press, Cambridge, 1977).
[31] H. W. Guggenheimer, *Differential Geometry* (McGraw-Hill, New York, 1963), p. 30.
[32] M. L. Kurnaz and D. K. Schwartz, Phys. Rev. E **56**, 3378 (1997).
[33] L. D. Landau and E. M. Lifshitz, *Theory of Elasticity*, 3rd ed. (Pergamon, Oxford, 1959).
[34] K. J. Stine and D. T. Stratmann, Langmuir **8**, 2509 (1992).
[35] S. Riviere, S. Henon, J. Meunier, D. K. Schwartz, M. W. Tsao, and C. M. Knobler, J. Chem. Phys. **101**, 10045 (1994).